Article

Cell Reports

Dnase2a Deficiency Uncovers Lysosomal Clearance of Damaged Nuclear DNA via Autophagy

Graphical Abstract

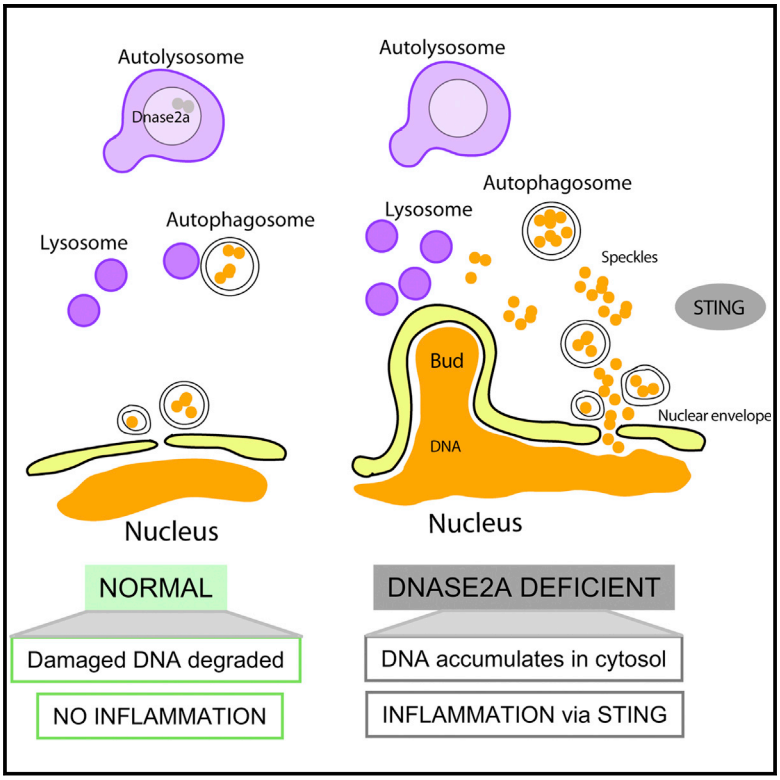

Highlights

Cells deficient for lysosomal Dnase2a or autophagy accumulate extranuclear DNA

Cells treated with DNA damaging agents also accumulate extranuclear DNA

Extranuclear DNA is found in buds or small speckles

Sting-mediated inflammation is induced by accumulated DNA

Authors

Yuk Yuen Lan, Diana Londoño, ..., Michael S. Rooney, Nir Hacohen

Correspondence

nhacohen@partners.org

In Brief

Deficiencies in DNA nucleases can lead to the accumulation of self DNA, activation of innate immunity, and development of autoimmune disease. The source of immunostimulatory DNA is not known in most cases. Lan et al. now find that damaged nuclear DNA accumulates outside the nucleus and stimulates *Sting*-dependent DNA-sensing when mice lack a lysosomal nuclease, *Dnase2a*. The results support a model in which damaged chromosomal DNA is normally exported from the nucleus and cleared by autophagy.

Lan et al., 2014, Cell Reports 9, 1–13
October 9, 2014 ©2014 The Authors
http://dx.doi.org/10.1016/j.celrep.2014.08.074

Please cite this article in press as: Lan et al., Dnase2a Deficiency Uncovers Lysosomal Clearance of Damaged Nuclear DNA via Autophagy, Cell Reports (2014), http://dx.doi.org/10.1016/j.celrep.2014.08.074

Cell Reports
Article

Dnase2a Deficiency Uncovers Lysosomal Clearance of Damaged Nuclear DNA via Autophagy

Yuk Yuen Lan,[1,2,3,6] Diana Londoño,[1,6,7] Richard Bouley,[4] Michael S. Rooney,[2,5] and Nir Hacohen[1,2,3,*]
[1]Center for Immunology and Inflammatory Diseases, Massachusetts General Hospital, 149 13th Street, Charlestown, MA 02129, USA
[2]Broad Institute, 415 Main Street, Cambridge, MA 02142, USA
[3]Department of Medicine, Harvard Medical School, Boston, MA 02115, USA
[4]Center for Systems Biology, Program in Membrane Biology and Nephrology Division, Massachusetts General Hospital, 185 Cambridge Street, Boston, MA 02114, USA
[5]Harvard/MIT Division of Health Sciences and Technology, Cambridge, MA 02139, USA
[6]Co-first author
[7]Present address: Department of Neurology, The Illinois Neurologic Institute, 530 Northeast Glen Oak Avenue, University of Illinois College of Medicine, Peoria, IL 61637, USA
*Correspondence: nhacohen@partners.org
http://dx.doi.org/10.1016/j.celrep.2014.08.074

SUMMARY

Deficiencies in DNA-degrading nucleases lead to accumulation of self DNA and induction of autoimmunity in mice and in monogenic and polygenic human diseases. However, the sources of DNA and the mechanisms that trigger immunity remain unclear. We analyzed mice deficient for the lysosomal nuclease *Dnase2a* and observed elevated levels of undegraded DNA in both phagocytic and nonphagocytic cells. In nonphagocytic cells, the excess DNA originated from damaged DNA in the nucleus based on colocalization studies, live-cell imaging, and exacerbation by DNA-damaging agents. Removal of damaged DNA by Dnase2a required nuclear export and autophagy-mediated delivery of the DNA to lysosomes. Finally, DNA was found to accumulate in *Dnase2a*$^{-/-}$ or autophagy-deficient cells and induce inflammation via the *Sting* cytosolic DNA-sensing pathway. Our results reveal a cell-autonomous process for removal of damaged nuclear DNA with implications for conditions with elevated DNA damage, such as inflammation, cancer, and chemotherapy.

INTRODUCTION

Mammalian cells express numerous nucleic sensors that detect and induce responses to invading viruses and other microbes (Barber, 2011; Paludan and Bowie, 2013). Although this suite of sensors can also recognize self DNA and RNA, several mechanisms are in place to avoid such innate immune responses to self. First, a subset of the RNA and DNA sensors—TLR3, 7, 8, and 9—are localized to endosomal compartments that appear to be spatially segregated from self nucleic acids (Ishii and Akira, 2006; Stetson and Medzhitov, 2006). For example, when TLR9 is engineered to localize on the surface of cells, it recognizes circulating DNA and induces inflammation (Barton et al., 2006). Second, self nucleic acids may have modifications that render them undetectable to some sensors (Iwasaki, 2012). Finally, nucleases clear cells of excess nucleic acids that might otherwise activate sensors. Evidence for this last mechanism is abundant, because mutations in DNases and RNases lead to autoimmunity in mouse models and in human monogenic and polygenic diseases.

Specifically, mutations in *Dnase1* (Napirei et al., 2000; Yasutomo et al., 2001), *Dnase2* (Kawane et al., 2006, 2010), and *Dnase3/Trex1* (Crow et al., 2006; Lee-Kirsch et al., 2007; Morita et al., 2004) enable self DNA originating from apoptotic cells (Yoshida et al., 2005) or retroelements (Stetson et al., 2008) to accumulate and results in autoimmune diseases, including systemic lupus erythematosus and Aicardi-Goutiéres syndrome in humans (Crow et al., 2006; Lee-Kirsch et al., 2007; Yasutomo et al., 2001), and autoimmune arthritis (Kawane et al., 2006, 2010), nephritis (Gall et al., 2012), and myocarditis (Morita et al., 2004) in mice. Studies of the *Trex1/Dnase3* gene that degrades DNA (Chowdhury et al., 2006; Mazur and Perrino, 2001) clearly demonstrate the consequences of cells overreacting to self DNA. *Trex1*$^{-/-}$ mice were shown to develop a lethal autoimmune cardiomyopathy (Morita et al., 2004) with associated accumulation of single-stranded DNA produced in S phase (Yang et al., 2007); subsequent studies implicated undegraded retroelements as a source of immunostimulatory DNA (Stetson et al., 2008) and demonstrated the importance of the *Sting* DNA-sensing pathway in triggering inflammation and autoimmunity (Gall et al., 2012).

Another example is *Dnase2a*, a ubiquitously expressed lysosomal DNA endonuclease that degrades DNA to oligonucleotides and nucleotides (Evans and Aguilera, 2003). *Dnase2a*$^{-/-}$ mice spontaneously produce high levels of type I interferons (IFNs) and show embryonic lethality that is rescued by removing the IFN receptor (Yoshida et al., 2005). Conditional ablation of *Dnase2a* in adult mice leads to production of immune cytokines (e.g., tumor necrosis factor [TNF-α], interleukin 6 [IL-6], CXCL10, IL-1β, and type I IFNs), autoantibodies (rheumatoid factor and anti-double-stranded DNA [dsDNA]) and development of chronic polyarthritis that resembles human rheumatoid arthritis (Kawane

Please cite this article in press as: Lan et al., Dnase2a Deficiency Uncovers Lysosomal Clearance of Damaged Nuclear DNA via Autophagy, Cell Reports (2014), http://dx.doi.org/10.1016/j.celrep.2014.08.074

et al., 2006). Consistent with the role of lysosomes in recycling materials ingested via endocytosis, undigested DNA (partly derived from discarded erythrocyte nuclei) was found in fetal liver macrophages in *Dnase2a* knockout mice (Kawane et al., 2001; Krieser et al., 2002).

These two models of DNase deficiency demonstrate that defective degradation of nucleic acids can activate autoimmune responses, and yet the source and mechanism of clearance of DNA remain unclear. We focused on the *Dnase2a*-knockout as a genetic model to dissect the source and subcellular localization of DNA and the mechanisms that trigger immunity and observed unexpected accumulation of nuclear DNA outside the nucleus. Additional experiments led us to define a mechanism by which lysosomal *Dnase2a* clears damaged nuclear DNA via autophagy.

RESULTS

DNA Accumulates in Phagocytic and Nonphagocytic *Dnase2a*-Deficient Cells

We hypothesized that phagocytic cells likely accumulate the highest levels of DNA in *Dnase2a*-deficient animals based on their ability to ingest erythrocyte nuclei and apoptotic cells (Krieser et al., 2002; Yoshida et al., 2005). Consistent with the hypothesis, we detected excessive DNA content in professional phagocytes (using propidium iodine [PI] and other DNA dyes such as Ruby and Hoechst), including bone-marrow-derived dendritic cells (BMDCs) and splenic DCs from *Dnase2a*$^{-/-}$ mice (Figure 1A), as well as primary BMDCs silenced for *Dnase2* by stably expressed small hairpin RNAs (shRNAs). To determine the distribution of DNA in these mice, we stained tissue sections with DAPI and observed higher levels of DNA in cells of joints, kidney and liver of knockout (*Dnase2a*$^{-/-}$) relative to wild-type (*Dnase2a*$^{+/+}$) mice (Figure 1B). Concomitant with the heightened inflammation previously observed in *Dnase2a*$^{-/-}$ mice, we detected elevated levels of inflammatory genes (the IFN-inducible chemokine, *Cxcl10* and the cytokines, *Il6* and *Tnfα*) in all cell types (B and T cells, DCs, macrophages) of the spleen from knockout mice relative to control littermates. This global activation could occur as a result of independent, autonomous events in each cell type or a cascade of inflammation initiated by a small number of cells.

We were surprised to observe increased DNA levels in nonphagocytic lymphocytes (primary T and B cells, Figure 1C; with the small fraction of genomic DNA representing a significant absolute level of DNA) and nonimmune cells, including primary lung and skin fibroblasts, long-term cultured mouse lung fibroblasts (MLFs), in knockout versus wild-type mice, and *p53*$^{-/-}$ mouse embryonic fibroblasts (MEFs) silenced with *Dnase2a*-targeting shRNAs (Figure S1A). To exclude the possibility that *Dnase2a*$^{-/-}$ cells are more often in S phase (>2n DNA) relative to wild-type cells, we synchronized nonphagocytic MLFs of both genotypes and observed a similar increase in DNA by PI staining (Figure 1D; Ruby staining showed same result). We also confirmed the higher DNA content in *Dnase2a*$^{-/-}$ cells with independent measurements, including UV absorbance of purified genomic DNA (Figure 1E), which correlated well with mean intensity of dye-stained cells by flow cytometry (Figure S1B). These results imply that *Dnase2a* is essential for preventing the accumulation of DNA, not only as expected in phagocytic cells, but also in nonphagocytic cells.

Damaged DNA Is Found outside the Nucleus of *Dnase2a*-Deficient Cells

We suspected that the excess DNA could be derived from an intracellular source. To pinpoint the location of accumulated DNA within *Dnase2a*-deficient cells, we stained MLFs with anti-dsDNA. We observed small and large DNA aggregates at perinuclear regions (Figure 2A, untreated), and interestingly, adjacent to condensed chromosomes of dividing cells (Figure S2A, untreated). We thus hypothesized that damaged chromosomal DNA would need to be discarded during replication or DNA damage and repair and exported from the nucleus for degradation by Dnase2a.

To visualize DNA fragments generated by damage or repair, we stained tissues and cultured cells for phosphorylated histone 2AX (γ-H2AX), an established marker of double-stranded DNA breaks (DSBs). In vivo staining of γ-H2AX was dramatically elevated in the kidneys of *Dnase2a*-deficient relative to wild-type mice (Figure 2B), and similarly in vitro in *Dnase2a*-deficient MLFs (Figure 2C, untreated), suggesting that damaged DNA accumulates to high levels in the absence of *Dnase2a* in the steady state. We also noted that there was increased nuclear DNA and γ-H2AX signal in the nucleus of *Dnase2a*$^{-/-}$ MLFs (Figures 2A, 2C, and 2D). Whether excess extranuclear DNA may hinder the export of damaged nuclear DNA and thus promote DNA damage in the nucleus is an open question.

To increase the burden of endogenous damaged DNA, we treated cells or mice with cytarabine (Ara-C), a nucleoside analog that causes replication stalls, and observed even higher levels of extranuclear DNA in cells (Figure 2A, treated), whereas cell viability remained high (Figure S2B). In addition, *p53*$^{-/-}$MEFs, which have defects in the regulation of DNA repair, showed clear dose-responsive DNA accumulation to Ara-C by flow cytometry and immunostaining (Figures S2C and S2D). Two different anti-dsDNA antibodies (sc-58749, DNA11-M) and serum from NZB/NZW lupus mice gave similar staining results. DAPI staining also showed similar patterns but required acetone fixation and did not reveal the small DNA speckles in the cytosol (Figure S2E). Preincubation with DNA, including salmon DNA, calf thymus DNA and IFN-stimulatory DNA (ISD), and digested with DNase I confirmed the specificity of the anti-dsDNA antibody (Figures S2F and S2G). We note that MLFs with excessive levels of damaged DNA did not detectably transfer their DNA to cells with normal levels of DNA after 24 hr of coculture, indicating that the observed extranuclear DNA aggregates were not derived from extracellular sources (Figure S2H).

Importantly, the γ-H2AX signal, which was higher in *Dnase2a*$^{-/-}$ cells after Ara-C treatment (Figure 2C, treated), co-localized with dsDNA both at perinuclear buds and cytosolic speckles (Figure 2D). Furthermore, in vivo treatment of Ara-C aggravated joint swelling in *Dnase2a*$^{-/-}$ mice suggesting that damaged DNA could exacerbate arthritis in this model (Figure 2E, we used younger animals at 4 months of age before development of arthritis). Thus, the extranuclear DNA accumulating in *Dnase2a*-deficient cells—spontaneously or induced by

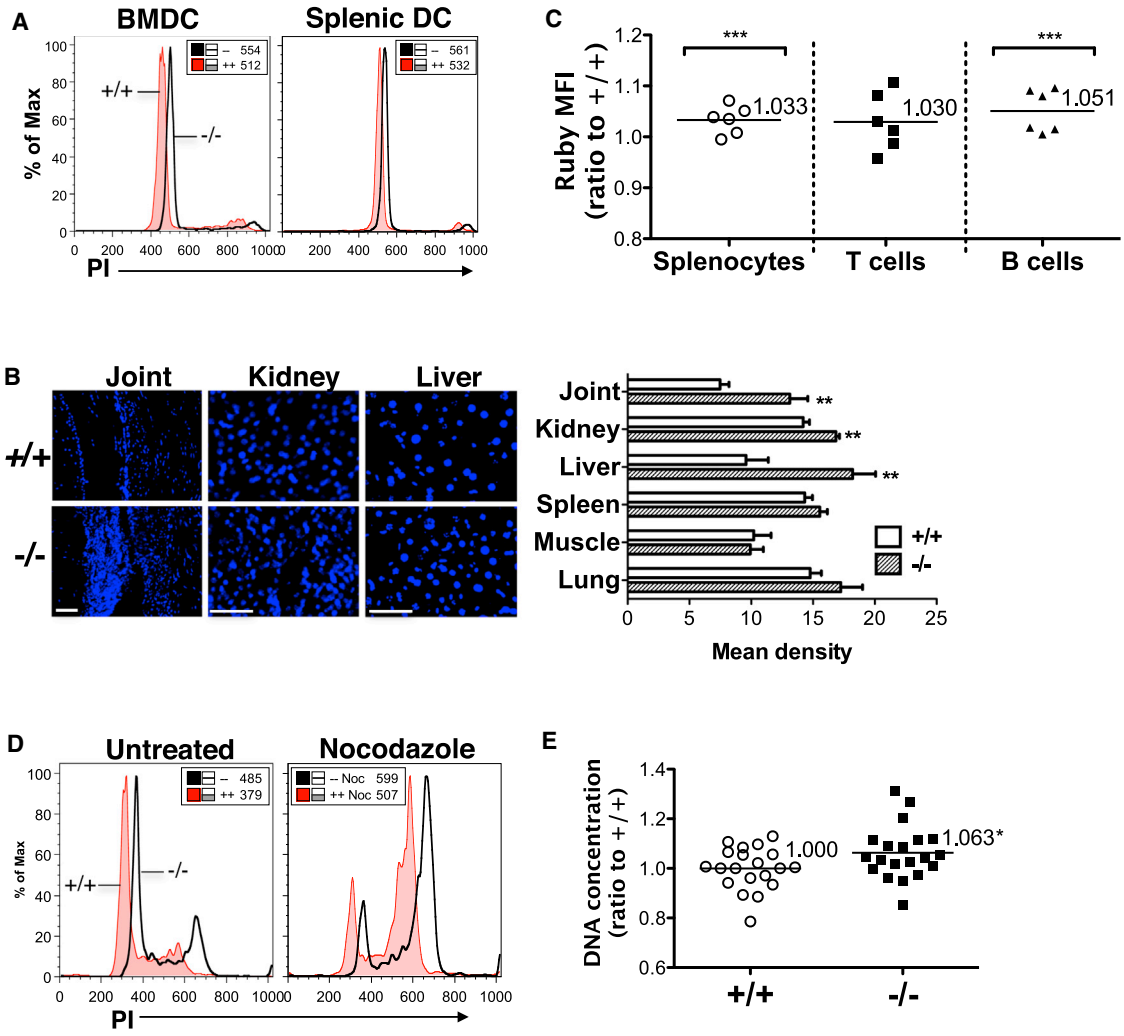

Figure 1. Accumulation of DNA in *Dnase2a*-Deficient Cells

(A) DNA content of BMDCs and splenic DCs from wild-type and *Dnase2a*$^{-/-}$ mice examined by PI staining (MFI shown), representative of three independent experiments with MFI ratio of *Dnase2a*$^{-/-}$ to *Dnase2a*$^{+/+}$ of 1.15 ± 0.13 SD (BMDCs) and 1.19 ± 0.24 SD (splenic DCs).

(B) DAPI staining of tissues from wild-type and *Dnase2a*-deficient mice. Mean density of DAPI-positive areas is based on five to ten total fields from two independent comparisons of matched wild-type and knockout mice; values are mean ± SEM; scale bar represents 10 μm.

(C) Overall DNA content of live immune cells from spleens of wild-type and *Dnase2a*-deficient mice assessed by flow cytometry using Ruby dye. Each symbol represents the ratio of the MFI from cells of *Dnase2a*$^{-/-}$ versus matched *Dnase2a*$^{+/+}$ mice. Six independent experiments were analyzed using a regression model to account for technical batch effect and biological variation; mean MFI ratios for all experiments per cell type are indicated next to the horizontal bars that mark the mean.

(D) DNA content of nocodazole-synchronized (100 ng/ml for 16 hr) *Dnase2a*$^{+/+}$ and *Dnase2a*$^{-/-}$ MLFs by PI staining, representative of three independent experiments with MFI shown, $p < 0.05$.

(E) Relative amount of purified genomic DNA content from *Dnase2a*$^{+/+}$ or *Dnase2a*$^{-/-}$ MLFs by UV absorbance. Each data point is the ratio of DNA from a single sample versus the mean of all *Dnase2a*$^{+/+}$ samples. Horizontal bars mark mean ratios.

See also Figure S1.

DNA-damaging agents—appears to consist of damaged dsDNA fragments.

Accumulated DNA Originates in the Nucleus

Supporting the nuclear origin of accumulated DNA, three major spatial patterns of extranuclear DNA were observed by confocal microscopy (Figure 3A, relative frequencies on the right): (1) nuclear buds that appear continuous with the nucleus (found in *Dnase2a*$^{-/-}$ but rarely in wild-type cells); (2) cytosolic speckles that fan out from the nucleus (most prominent upon Ara-C treatment); and (3) large extranuclear aggregates that are likely to be detached nuclear buds based on their shape, size, and proximity to the nucleus (mostly in Ara-C-treated cells). High-resolution fluorescence and electron microscopy staining for dsDNA further confirmed the presence of DNA buds and speckles (emanating at specific points) in close apposition with the

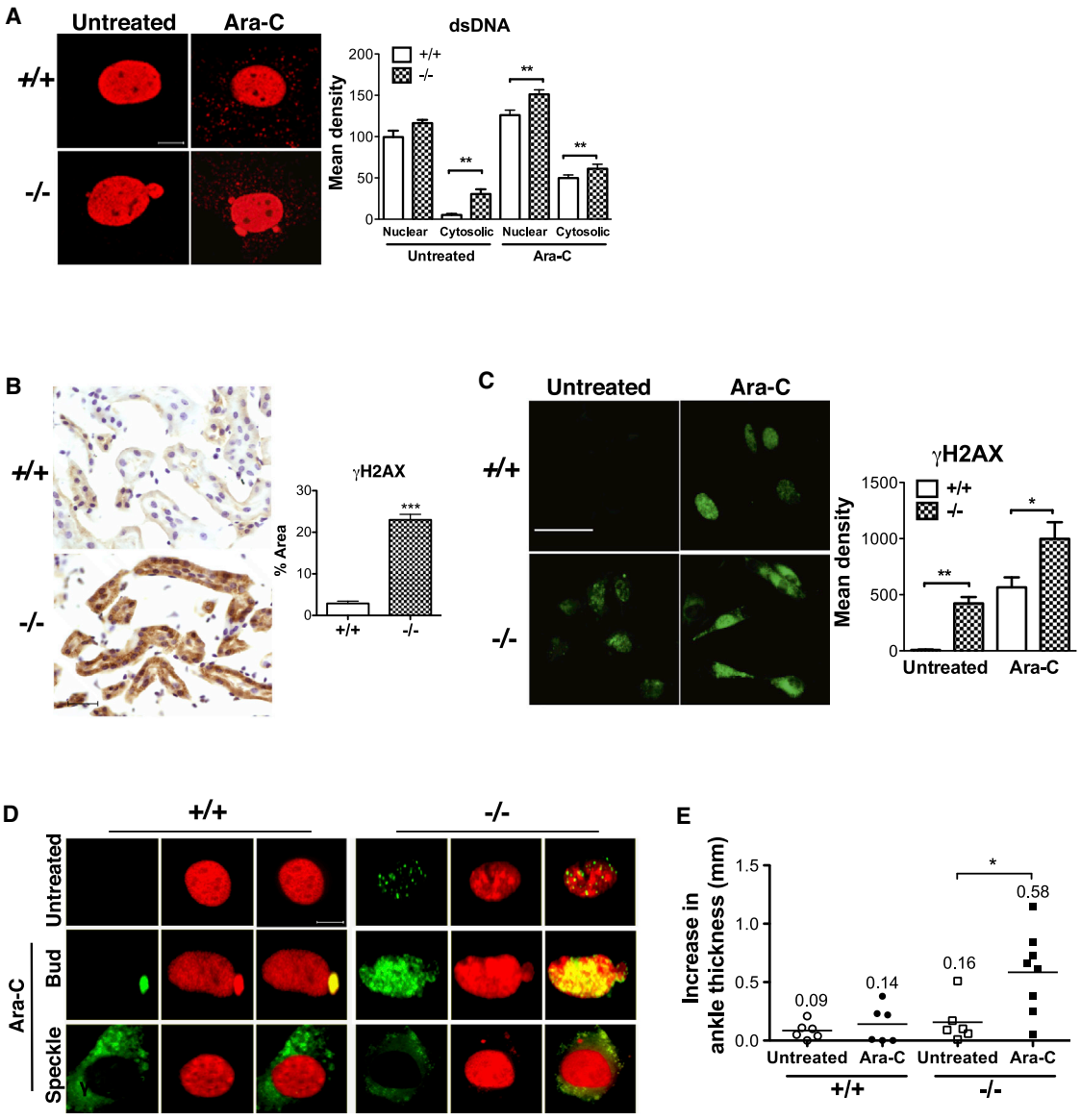

Figure 2. Damaged DNA in the Cytosol of *Dnase2a*-Deficient Cells

(A) Fluorescent staining of MLFs from wild-type or *Dnase2a*$^{-/-}$ mice with anti-dsDNA; scale bar represents 10 μm. Right, quantitation of dsDNA in nuclear and cytosolic compartments based on five total fields of 20× from three independent experiments.

(B) Immunoperoxidase staining of anti-γ-H2AX in kidneys of wild-type and *Dnase2a*$^{-/-}$ mice, scale bar represents 10 μm; right, quantitation of signals as percentage total area based on five fields of 20× from three matched pairs of wild-type and *Dnase2a*$^{-/-}$ mice.

(C) Immunofluorescent staining of anti-γ-H2AX in MLFs, scale bar represents 50 μm; right, quantitation of signals as mean density based on five fields of 20× from three independent experiments.

(D) Double-staining with anti-γ-H2AX (green) and anti-dsDNA (red) in MLFs; yellow indicates colocalization; scale bar represents 10 μm; images representative of three independent experiments.

(E) Increase in ankle thickness from week 0 to week 8 (for both ankles) in matched 10- to 12-week-old wild-type and *Dnase2a*$^{-/-}$ mice (n = 3-4), untreated or injected with three doses of 15 μg/g Ara-C i.p., mean increase is shown numerically.

Values in (A)–(C) are mean ± SEM. See also Figure S2.

nucleus (Figure 3B). Buds and speckles were often encircled by or colocalized with the nucleoporin protein, NUP98, a docking site for transport at the nuclear pore complex and marks the nuclear envelope (Figure 3C). When the fate of newly synthesized nuclear DNA was tracked with bromodeoxyuridine (BrdU), we observed comparable patterns of perinuclear buds and cytosolic speckles emanating from the nucleus (Figure 3D), indicating that replicated DNA contributed to extranuclear DNA.

We tested the potential of mitochondria to contribute excess DNA, and found that MitoTracker signal (Figure S3A) and

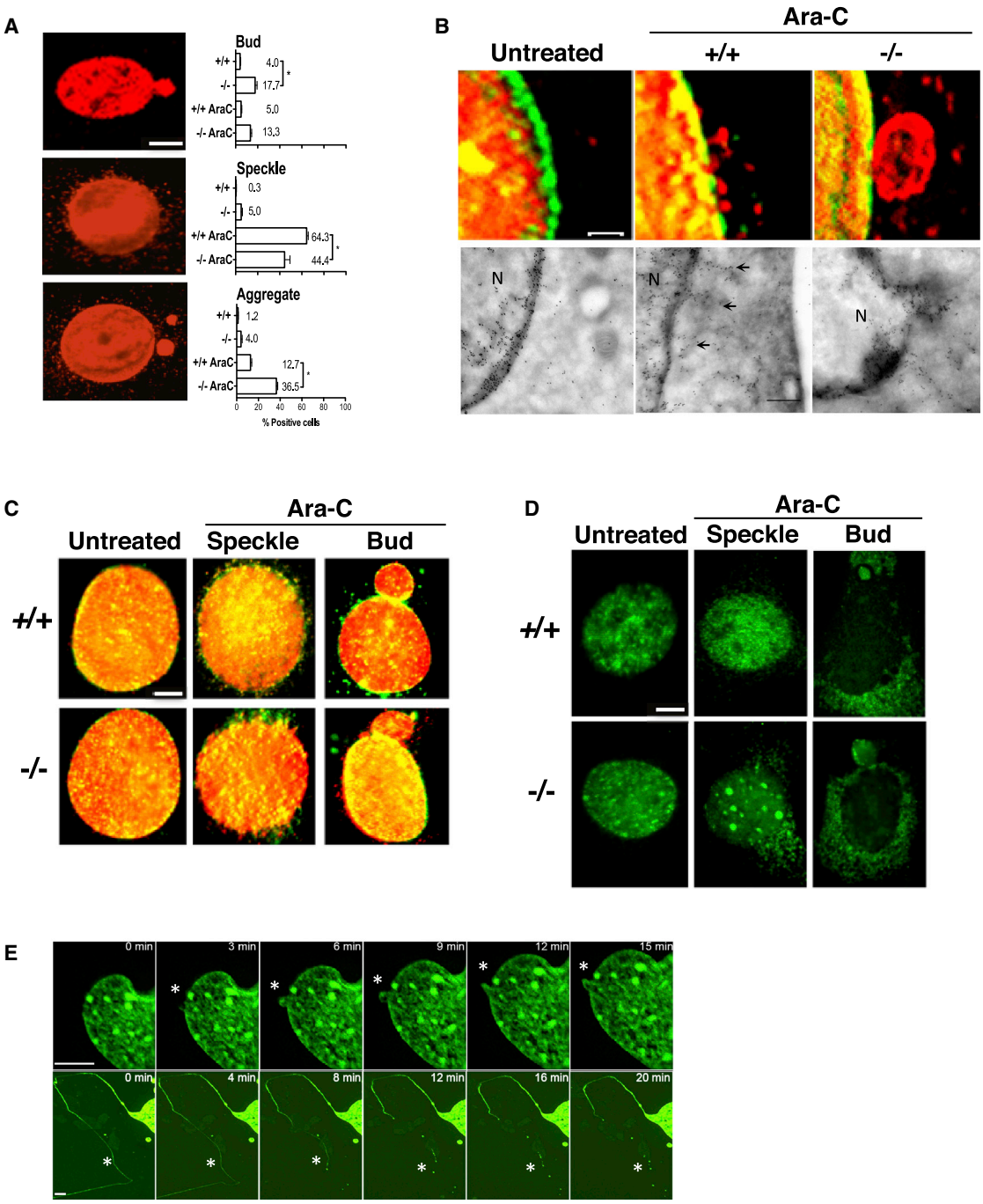

Figure 3. Export of DNA from Nucleus to Cytosol

(A) Left, immunostaining of anti-dsDNA shows three distinct extranuclear DNA patterns quantified in MLFs: nuclear buds, cytosolic speckles, large extranuclear aggregates; scale bar represents 10 μm. Right, frequencies in *Dnase2a*$^{+/+}$ and *Dnase2a*$^{-/-}$ MLFs, without or with Ara-C treatment (10 μM, 24 hr), based on ten fields at 20×. Values are mean ± SEM. Frequency of normal nuclei is not shown.

(B) Representative images of immunofluorescence staining (anti-NUP98, green; anti-dsDNA, red; scale bar represents 2 μm) and electron microscopy (immunogold anti-dsDNA; scale bar represents 500 nm; N, nucleus) in MLFs. Untreated cell with clear cytoplasm is a *Dnase2a*$^{+/+}$ MLF.

(C) Anti-dsDNA (red) and anti-NUP98 (green) staining in MLFs; scale bar represents 10 μm.

(D) MLFs pulsed with BrdU (15 μM for 6 hr) show newly replicated DNA in buds and speckles; scale bar represents 10 μm.

(E) Sequences from time-lapse imaging of GFP-H2B-infected MLFs illustrating nuclear DNA budding (top series) and thread formation/detachment (bottom series); scale bar represents 5 μm; asterisks highlight changes.

See also Figure S3 and Movies S1 and S2.

Please cite this article in press as: Lan et al., Dnase2a Deficiency Uncovers Lysosomal Clearance of Damaged Nuclear DNA via Autophagy, Cell Reports (2014), http://dx.doi.org/10.1016/j.celrep.2014.08.074

PCR-based quantitation of mitochondrial DNA (Figure S3B) was not significantly different between *Dnase2a*$^{+/+}$ and *Dnase2a*$^{-/-}$ cells. Only a minor fraction of extranuclear DNA colocalized with mitochondria by immunofluorescence (Figure S3C). To further exclude mitochondria as a source of DNA, we used aphidicolin to inhibit nuclear but not mitochondrial replication (Ikegami et al., 1978) and observed abrogation of the cytosolic DNA accumulation in the presence of Ara-C (Figure S3D). The observations of dsDNA accumulation along with experiments excluding mitochondria indicate that the nucleus is the major source of accumulated DNA in *Dnase2a* knockout and Ara-C-treated cells.

DNA Is Exported from Nucleus

To study the spatial and temporal dynamics of excess DNA, we infected wild-type and *Dnase2a*$^{-/-}$ MLFs with a retrovirus carrying GFP-H2B. Although DNA dyes (e.g., Hoechst and Ruby) induce phototoxicity and limit their use for live capture, histone proteins are known to associate tightly with DNA and have been used as surrogate markers for DNA (Kanda et al., 1998). We confirmed the colocalization of GFP-H2B with dsDNA in the cytosol by immunofluorescence (Figure S3E). Time-lapse live imaging of Ara-C-treated cells with a spinning disc confocal microscope revealed several steps of the nuclear DNA export process, including nuclear DNA bud formation and detachment of nuclear DNA from the nucleus into the cytosol (through unusual thread-like structures that are first connected to the nucleus and then fragment in the cytosol) after 2–8 hr of Ara-C treatment (Figure 3E; Movies S1 and S2). These live observations demonstrate that endogenous DNA moves out of the nucleus when cells are under genotoxic stress.

Accumulated DNA Induces Inflammation

The abnormally high level of damaged DNA outside the nucleus has the risk of activating innate immune DNA-sensing pathways that induce cytokine and chemokines. Indeed, Ara-C as well as topoisomerase inhibitors (doxorubicin and etoposide that act through independent mechanisms) not only caused a rise in DNA levels but also upregulated chemokine and cytokine gene expression (including *Cxcl10*, *Ifnb*, *Il6*, *Tnfa*) in a dose-dependent manner in *p53*$^{-/-}$ MEFs (data not shown). In MLFs, we found that the upregulation of *Cxcl10* expression as a result of Ara-C treatment was most pronounced when *Dnase2a* was absent (Figure 4A). Confirming that the excessive DNA and *Cxcl10* levels observed in *Dnase2a*$^{-/-}$ MLFs were indeed due to lack of degradation by Dnase2a, we successfully rescued the inflammatory and extranuclear DNA phenotypes with inducible *Dnase2a* expression (*Cxcl10*, Figure 4B; dsDNA, Figure 4C). Furthermore, the known adaptor *Sting*/*Tmem173* and mediator *Tbk1* of the cytosolic DNA-sensing pathway, were expressed at higher levels in knockout compared to wild-type MLFs (Figure S4A), and small interfering RNA (siRNA)-mediated silencing of either mediator abolished the heightened immune activation observed in *Dnase2a*-deficient and Ara-C-treated cells (Figure 4D), consistent with loss of arthritis in *Dnase2a*$^{-/-}$*Sting*$^{-/-}$ mice (Ahn et al., 2012). Finally, corroborating the nuclear origin of the accumulated DNA, inhibition of nuclear export by leptomycin B (LMB) almost completely abolished cytokine production (Figure 4E) in MLFs, whereas ISD-induced *Cxcl10* expression was only partially reduced (Figure S4B). Thus, exported nuclear DNA that accumulates as a result of a *Dnase2a* deficiency or induction of DNA damage engages a *Sting*-dependent cytosolic nucleic acid sensing pathway to induce inflammation.

DNA Localizes with Autophagosomes and Lysosomes

Given that Dnase2a colocalizes with DNA in a LAMP1^{+} compartment, a key question is how extranuclear DNA is transported to the lysosome for degradation by Dnase2a. We considered the possibility that autophagy, a major mechanism for recycling of cytosolic cargo, would deliver the excess DNA to lysosomes. Indeed, canonical autophagy genes, including *Atg5*, *Atg7*, and *Beclin1*, were significantly upregulated in *Dnase2a*-deficient MLFs compared with wild-type cells (Figure 5A). The autophagosomal marker LC3-II and the lysosomal protein LAMP1 were also elevated in *Dnase2a*$^{-/-}$ and Ara-C-treated MLFs (Figures 5B and 5C) and in *Dnase2a*$^{-/-}$ kidneys (Figure 5D) compared with those in wild-type. LC3 formed the typical punctate cytosolic pattern found during active autophagy.

To further visualize the overlap of autophagosomes and lysosomes with cytosolic DNA in the DNA degradation process, we used antibodies against LC3 and LAMP1 to study their colocalization with dsDNA. In Ara-C-treated wild-type cells, excess DNA colocalized with LC3 and LAMP1, likely reflecting autophagosome-lysosome fusion and the depositing of nuclear DNA into the lysosomal degradation pathway (Figure 5E, top, seen also in untreated wild-type cells [left], but this is a rare event). Confirming our findings, we note that the nucleocytoplasmic distribution of LC3 that we observe has been reported (Drake et al., 2010) and that GFP-LC3 showed similar intensity, punctate pattern, and colocalization with DNA (Figures S5A and S5B). In contrast, in *Dnase2a*-deficient MLFs, DNA aggregates did not localize with LAMP1 yet remained localized with LC3 (Figure 5E, bottom; also Figure S5C showing enlarged nuclear buds, and reduced DNA/LAMP1 and LC3/LAMP1 colocalization in Figure 5F). We suspect that aborted fusion may be a quality-control mechanism for avoiding lysosomes that lack degradation enzymes and results in accumulation of autophagosomes similar to what is observed in lysosomal storage disorders lacking hydrolases (Settembre et al., 2008).

Requirement for Autophagy and Lysosomes in Autonomous DNA Removal

Based on these data, we predicted that a defect in autophagy, like a deficiency in *Dnase2a*, would lead to elevated levels of DNA in the cell. We found that *Atg5*$^{-/-}$ MEFs amassed higher levels of DNA (Figure 6A, Ruby staining; Figure 6B, anti-dsDNA immunostaining), with elevated cytosolic speckles and aggregates (Figure 6C), but lacked colocalization of DNA with lysosomes (Figure 6D). Consistent with a role for autophagy in removing immunostimulatory DNA that could engage cytosolic DNA sensing pathways, basal increase of DNA levels in *Atg5*$^{-/-}$ MEFs was sufficient to mount an immune response, whereas Ara-C treatment heightened the level of cytokine expression (Figure 6E).

To test the role of the lysosome in DNA clearance, we blocked vesicular fusion to lysosomes using bafilomycin A1 (which

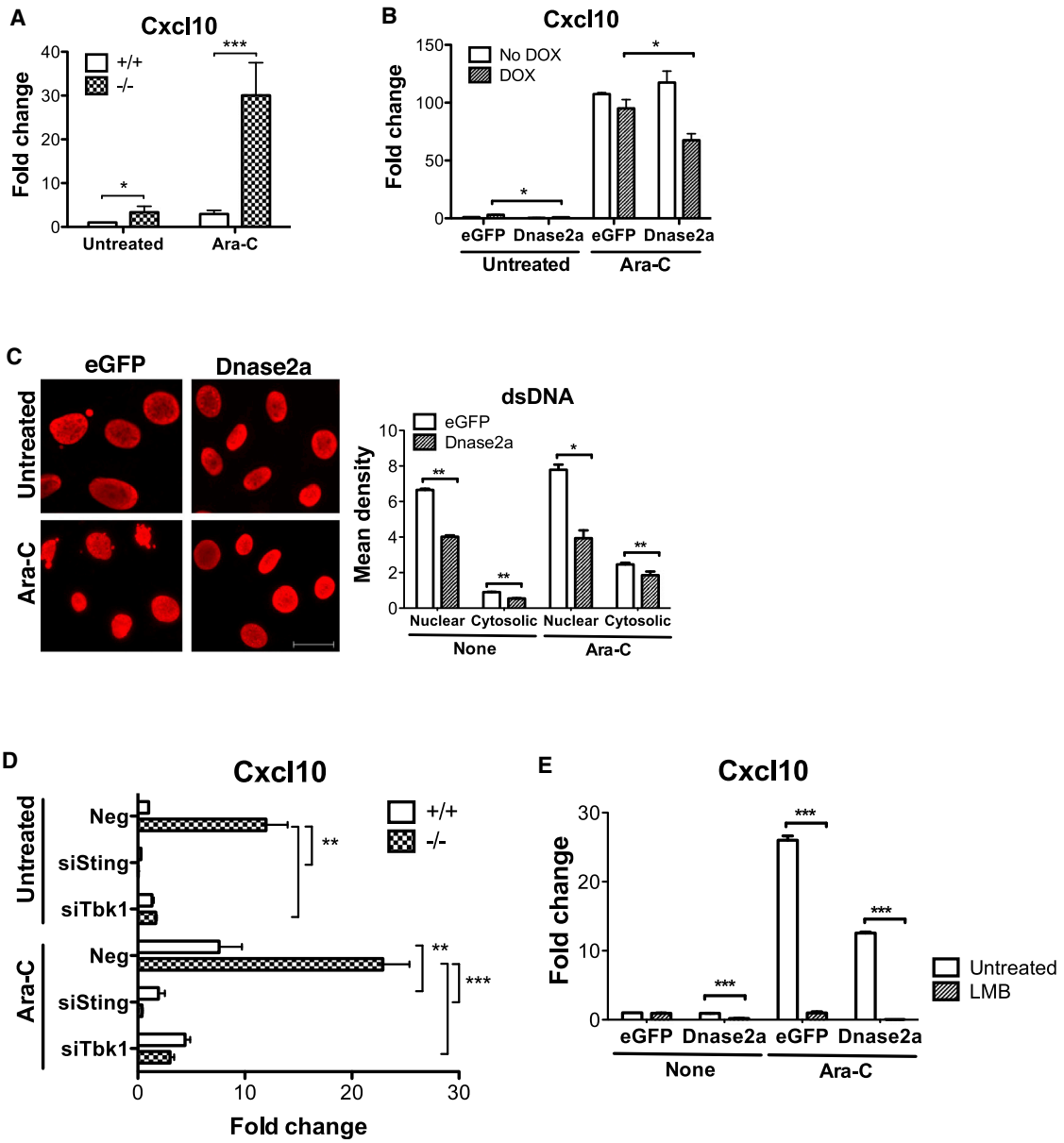

Figure 4. Accumulated DNA Activates Sting-Dependent Inflammation

(A) Expression of *Cxcl10* mRNA in untreated or Ara-C-treated wild-type and *Dnase2a*$^{-/-}$ MLFs.

(B) *Cxcl10* expression of *Dnase2a*$^{-/-}$ MLFs rescued with *Dnase2a* ORF using a Tet-on vector with doxycycline induction (3 μg/ml, 24 hr); *eGFP* ORF was used as negative control.

(C) Immunostaining of anti-dsDNA for KO and rescued cells (as in B); scale bar represents 20 μm; right, quantitation of fluorescent signals based on five fields of 20×.

(D) *Cxcl10* mRNA levels in *Dnase2a*$^{+/+}$ and *Dnase2a*$^{-/-}$ MLFs transfected with siRNAs targeting *Sting* or *Tbk1*, untreated or treated with 10 μM Ara-C for 24 hr.

(E) *Cxcl10* expression of KO or rescued MLFs after doxycycline induction, untreated or treated with Ara-C and leptomycin (20 nM, 24 hr) as indicated.

Values are mean ± SEM. Data are representative of two (B–D) or three (A and E) independent experiments. See also Figure S4.

inhibits V-ATPases and lysosomal acidification) and found enhanced accumulation of extranuclear DNA in wild-type MLFs treated with Ara-C (Figure S6). In contrast, the autophagy inducer rapamycin reduced the levels of cytosolic DNA in knockout cells (Figure S6). These data reveal a nuclear-to-autophagosome-to-lysosome transport pathway that targets nuclear DNA for degradation and is upregulated in the context of DNA damage. We note that silencing *Atg5* resulted in elevated DNA levels and *Cxcl10* expression that were beyond those observed in the *Dnase2a*$^{-/-}$ cells (Figure 6F). The synergistic phenotype of *Atg5*/*Dnase2a* deficient cells suggests the existence of additional autophagy-dependent mechanisms of DNA clearance

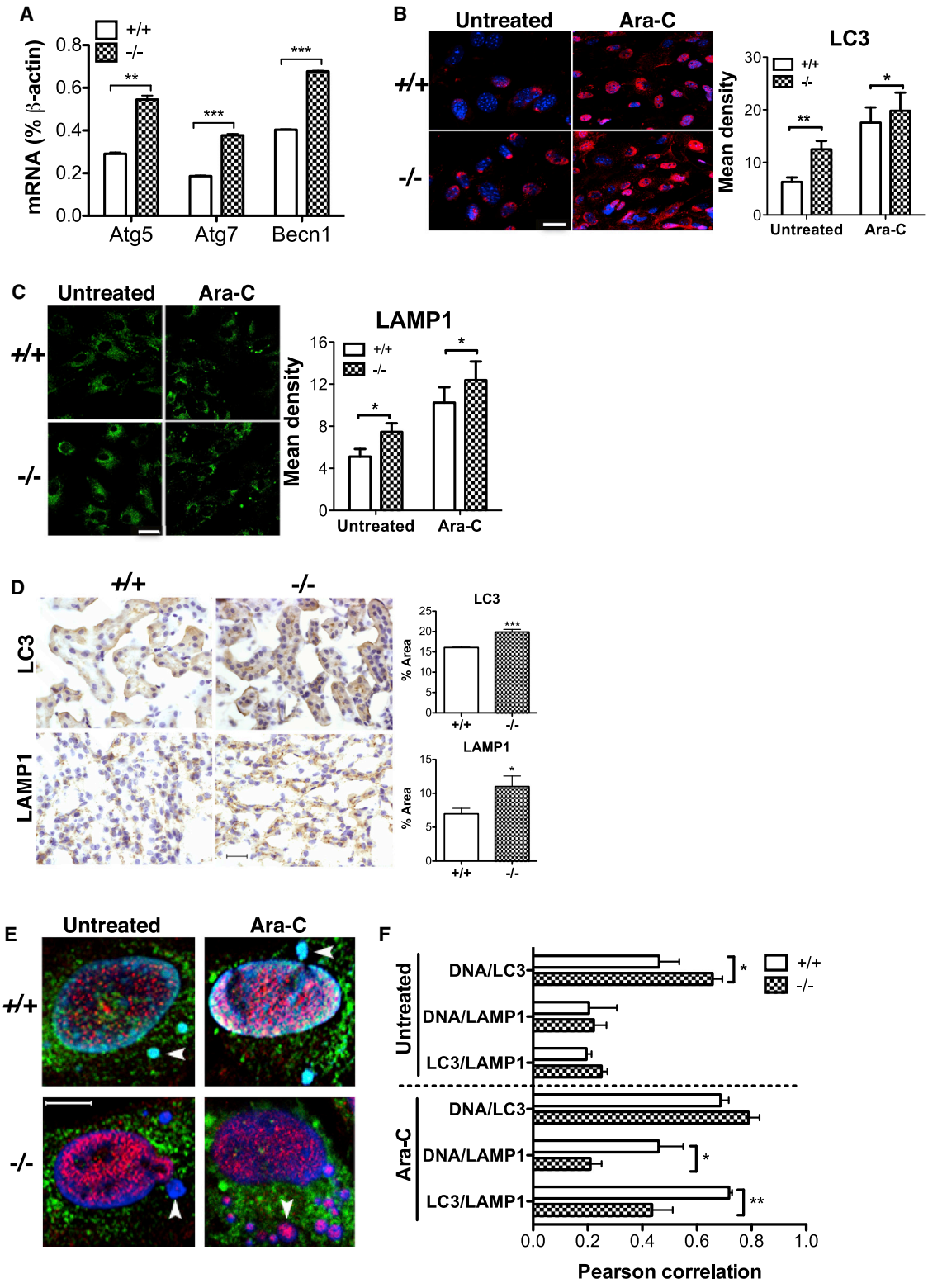

Figure 5. Autophagy in *Dnase2a* Deficiency

(A) Levels of autophagy gene mRNAs in wild-type and *Dnase2a*$^{-/-}$ MLFs.

(B) Immunostaining with anti-LC3 (red) in *Dnase2a*$^{+/+}$ and *Dnase2a*$^{-/-}$ MLFs showing punctate patterns, DAPI (blue) as counterstain; scale bar represents 10 μm; right, quantitation of LC3 signal.

(legend continued on next page)

beyond *Dnase2a*. Importantly, double knockdown of *Atg5* with *Sting* or *Tbk1* eliminated the immune response (Figure 6F), consistent with a role for STING in sensing damaged DNA (and its observed association with autophagosomes in the presence of DNA [Saitoh et al., 2009; Watson et al., 2012]).

DISCUSSION

An important question in immunology is whether self DNA can trigger the normal viral sensing pathways, and, if it does, what is the source of self DNA. We addressed these questions using *Dnase2a*$^{-/-}$ mice that develop arthritis and accumulate self DNA. Previous studies show that *Dnase2a* degrades DNA from ingested apoptotic cells (Kawane et al., 2001) and can even degrade entire genomes autonomously when cells die during development in fly (Bass et al., 2009). In contrast, our study focuses on an unexpected process by which lysosomal *Dnase2a* autonomously degrades damaged DNA that is exported from the nucleus in living cells (schematic in Figure S7).

In our study, we provide multiple lines of evidence that excess DNA in *Dnase2a*-deficient cells consists of exported nuclear DNA fragments. An important question is why the presence of extranuclear DNA has not been reported more regularly. We hypothesize that Dnase2a removes the exported DNA rapidly—before it can be visualized—analogous to the historical difficulties in observing apoptotic cells in animals due to their immediate removal by phagocytic cells. The observation of increased buds at the nuclear envelope in Dnase2a-deficient cells may thus indicate a higher rate of damaged DNA generation than removal. Nevertheless, other studies have detected DNA fragments arising from replication in budding yeast (Sogo et al., 2002) and fly (Blumenthal and Clark, 1977), overrepresented dsDNA fragments from chromosomes as free dsDNA molecules in human cells during S phase (Gómez and Antequera, 2008), and release of short DNA fragments into the cytosol prompted by physical (Kawashima et al., 2011) or radiation-induced injury (Pang et al., 2011). Interestingly, unrepaired or irreparable DNA has been found to relocalize to the nuclear periphery (Nagai et al., 2008; Oza et al., 2009), suggesting that it may be segregated from replicating DNA for clearance. These studies—along with those in *Trex1*$^{-/-}$ cells (Stetson et al., 2008; Yang et al., 2007)—are consistent with our findings.

Testing the in vivo impact of autonomous damaged DNA on inflammation is not feasible at this time because we cannot eliminate the effects of extracellular DNA in animals. However, prior studies of DNA repair gene KO models, in which generation of damaged DNA is elevated, are consistent with our cellular model. For example, *ATM*$^{-/-}$ cells accumulate cytoplasmic double-strand telomeric DNA in mouse and human cells (Hande et al., 2001), and *Atm*$^{-/-}$ and *p53*$^{-/-}$ MEFs show increased basal interferon-stimulated genes (ISGS) (Sugihara et al., 2011). Furthermore, p53 has been strongly implicated in autoimmune suppression, and its overexpression limits arthritis development through STAT-mediated regulation (Park et al., 2013). A more detailed analysis of the excess DNA in *Dnase2*$^{-/-}$ cells will be informative for tracing the chromosomal origin of the observed damaged DNA fragments (e.g., to mutation-prone common fragile sites [Ozeri-Galai et al., 2012], or early replication fragile sites [Barlow et al., 2013], regions of increased synthesis at rereplication sites [Green et al., 2010], or nucleosome-free gaps [Gómez and Antequera, 2008]).

We also observed that extranuclear DNA localizes in small speckles and large buds/aggregates and is often associated with the nuclear envelope. Furthermore, these structures colocalized with the autophagy machinery that is required for their clearance. These steps resemble the recently described phenomenon of nucleophagy (by which autophagy removes pieces of the nucleus [Mijaljica et al., 2010]), which is best described in yeast where piecemeal microautophagy of the nucleus pinches and degrades nuclear components in rapidly dividing cells, a process often induced by nutrient deprivation or rapamycin treatment (Krick et al., 2008; Roberts et al., 2003). Other examples include whole-nuclei removal in fungi (Shoji et al., 2010) as well as micronuclei in human cancer cells (Rello-Varona et al., 2012). In humans, nuclear laminopathies (caused by mutations in *Lmna*, encoding lamin A and C that form the structural support of the nucleus) and envelopathies (caused by mutations in *emerin*, a transmembrane protein on the inner nuclear membrane binding to lamin) (Dauer and Worman, 2009) show resemblance to our cellular observations—in cells with mutations in lamin A, giant perinuclear autophagosomes, or autolysosomes containing DNA form apparently because of loss of integrity in the nuclear structure and extrusion of damaged nuclei into the cytoplasm (Park et al., 2009). Nucleophagy has not been dissected in detail in mammals, and its exact relationship to our findings is not known (Mijaljica et al., 2010). Finally, a recent study reports that γ-H2AX-positive cytosolic chromatin fragments are processed by autophagy in senescent cells (Ivanov et al., 2013).

Our observation that undigested DNA is not present in lysosomes of Dnase2a KO cells indicates an additional regulatory step controlling the trafficking (Cai et al., 2007) and fusion of autophagosomes to lysosomes (e.g., analogous to lack of accumulated products in lysosomes in the absence of lysosomal hydrolases (Settembre et al., 2008). More importantly, how autophagy and the DNA sensing pathway interact requires further studies. A recent report that finds increased radiosensitivity of ATG5 or BCN1-depleted cells and reduced ATG5$^{-/-}$ tumor growth after irradiation (Ko et al., 2014) may be related to our finding that autophagy affects trafficking of damaged DNA. Furthermore, the ATG5 locus has been shown to affect susceptibility to lupus (Delgado-Vega et al., 2010; Graham et al., 2009; Kaiser and

(C) Immunostaining with anti-LAMP1 in *Dnase2a*$^{+/+}$ and *Dnase2a*$^{-/-}$ MLFs; scale bar represents 10 μm; right, quantitation of LAMP1 signal.
(D) Expression of LC3 and LAMP1 in kidneys of wild-type and *Dnase2a*$^{-/-}$ mice by immunoperoxidase detection and counterstained by hematoxylin, scale bar represents 10 μm; quantitation in percentage total area based on six random fields at 20×.
(E) Three-color confocal staining with anti-dsDNA (blue), anti-LC3 (red), and anti-LAMP1 (green) in wild-type and *Dnase2a*$^{-/-}$ MLFs (arrowheads indicate extranuclear DNA aggregates); scale bar represents 10 μm.
(F) Quantitation of overlap between pairs of stains (from experiment in E).
Quantitation of fluorescent signals in (B), (C), and (E) is based on five fields at 20× of duplicate experiments. Values are mean ± SEM. See also Figure S5.

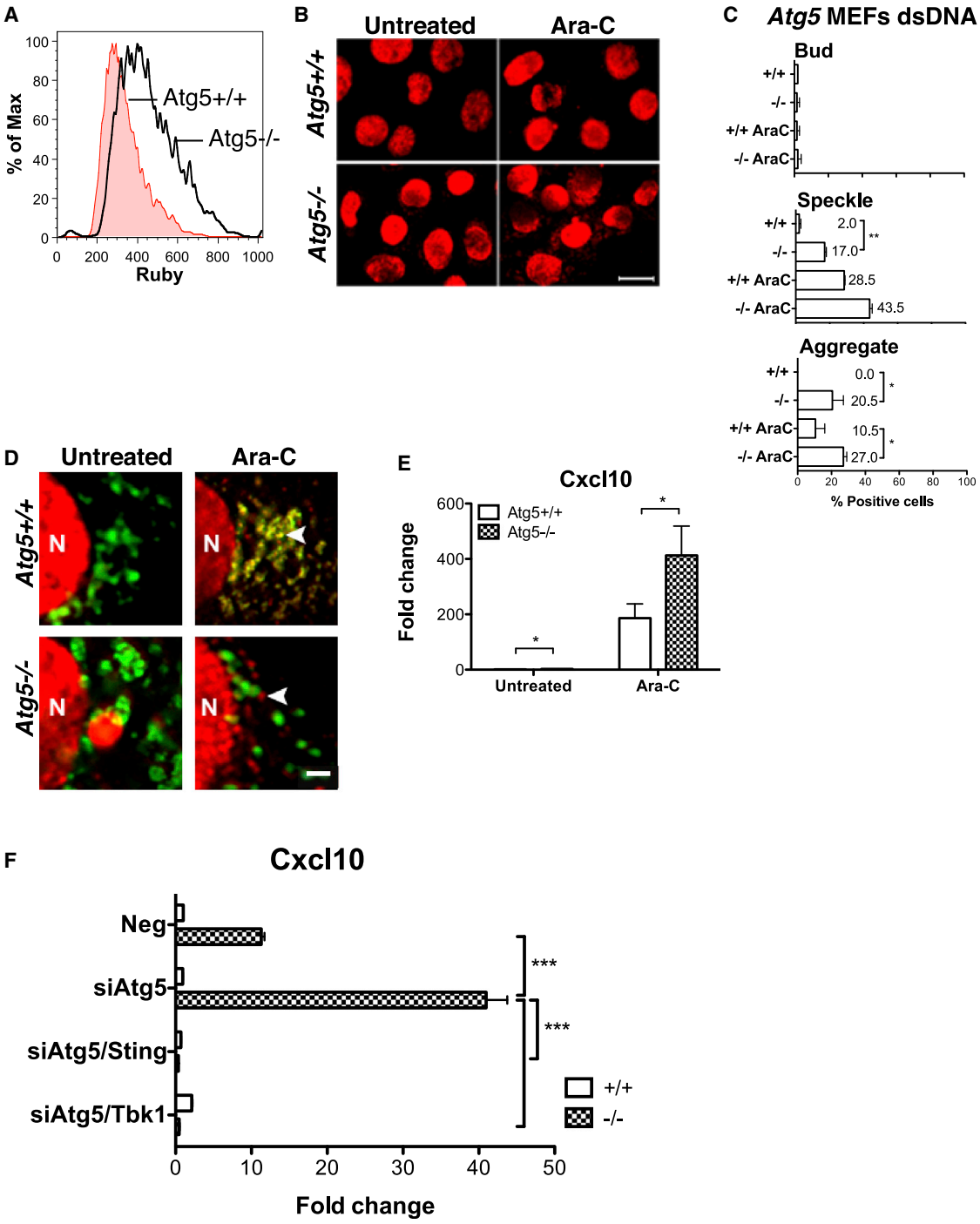

Figure 6. Role of Autophagy and Lysosomes in Autonomous DNA Removal

(A) DNA content of *Atg5*$^{+/+}$ and *Atg5*$^{-/-}$ MEFs by Ruby staining.

(B) Immunostaining of anti-dsDNA in *Atg5*$^{+/+}$ versus *Atg5*$^{-/-}$ MEFs with or without Ara-C treatment; scale bar represents 20 μm.

(C) Relative frequencies of bud, speckle, and aggregate patterns in *Atg5*$^{+/+}$ and *Atg5*$^{-/-}$ MEFs.

(D) Anti-LAMP1 (green) and anti-dsDNA (red) dual staining in *Atg5*$^{-/-}$ MEFs versus *Atg5*$^{+/+}$ cells; scale bar represents 2 μm; N, nucleus.

(E) Ratio of *Cxcl10* mRNA levels in *Atg5*$^{+/+}$ versus *Atg5*$^{-/-}$ MEFs with or without Ara-C treatment.

(F) Relative *Cxcl10* expression in wild-type or *Dnase2a*$^{-/-}$ MLFs silenced with siRNAs.

All data are results of independent duplicate experiments. Values are mean ± SEM. See also Figure S6.

Criswell, 2010), suggesting that perhaps the risk allele causes patient cells to amass DNA and induce excessive inflammation.

Prior studies have shown that ATM and NF-κB are critical in the induction of inflammation by DNA damage (Hinz et al., 2010; Yang et al., 2011) and that damaged DNA appears to stimulate the type I IFN response (Brzostek-Racine et al., 2011). Here, we add to these mechanistic studies by showing a requirement for *Sting* and *Tbk1* in the induction of inflammation in response to excess damaged DNA (consistent with *Dnase2a*$^{-/-}$*Sting*$^{-/-}$ mice not developing arthritis [Ahn et al., 2012]). Surprisingly, recent studies have found that DNA damage response (DDR) components Mre11 (Kondo et al., 2013), DNA-PK (Ferguson et al., 2012), and Ku70 (Zhang et al., 2011) (as well extrachromosomal histone H2B [Kobiyama et al., 2010]) are also required for induction of the cytosolic DNA-sensing pathway. Interestingly, some of the DNA repair proteins have also been found to be cleared by autophagy after DSB repair (Robert et al., 2011), suggesting that DDR proteins may bind the exported DNA fragments we observe and perhaps play a role in their stabilization, transport, and immune sensing. Together, these results point to an interesting yet poorly understood pathway that links damaged DNA, DNA repair proteins, and the innate immune response.

Why are there many nucleases involved in clearance of self DNA? It is likely that they specialize by targeting particular substrates within different subcellular compartments. For example, *Dnase2a* and *Trex1* are both critical nucleases that prevent cells from accumulating self DNA and triggering autoimmunity. Although deficiencies in either nuclease lead to *Sting*-dependent autoimmunity (Ahn et al., 2012; Gall et al., 2012), Trex1 associates with cytosolic face of the ER and targets single-stranded DNA (ssDNA), whereas Dnase2a sits in the lysosome and degrades dsDNA. Interestingly, a recent study observed upregulation of lysosomes in *Trex1*$^{-/-}$ cells (Hasan et al., 2013), suggesting that excess DNA may be triggering autophagy/Dnase2a-mediated clearance to compensate for lack of *Trex1*. Trex1 is able to degrade retroelement ssDNA (Stetson et al., 2008); however, consistent with the role of Dnase2a in degrading dsDNA, our preliminary deep sequencing of cytosolic DNA from *Dnase2*$^{-/-}$ cells did not show enrichment of retroelements (e.g., SINE, LINE, LTR sequences). Thus, whereas both nucleases are equally important for homeostasis, their DNA substrates, localization, and impact on disease appear to be distinct.

Finally, some of our findings may help explain the therapeutic effect of DNA-damaging agents in cancer. Such agents have been found to induce antitumor immunity (Galluzzi et al., 2012), and in other studies to activate the IFN-β-Stat1-ISG axis (Brzostek-Racine et al., 2011; Novakova et al., 2010). Our results suggest that the damaged DNA induced by these treatments would be exported from the nucleus and engage innate immune sensing pathways that could modulate tumor immunity.

EXPERIMENTAL PROCEDURES

Mice

Dnase2a$^{flox/-}$ and *Mx1-Cre* mice, a gift from Dr. Shigekazu Nagata (Kyoto University, Japan), were bred and genotyped to obtain conditional *Dnase2a*$^{flox/-}$*Mx1-Cre* mice. Wild-type littermates with matched age and sex were selected as controls. Both genotypes were injected intraperitoneally (i.p.) with 1.5 μg/weight (g) of poly I:C three times every other day at 12–16 weeks of age to induce deletion of *Dnase2a* as described (Kawane et al., 2006). Mice were housed in a specific pathogen-free facility at MGH, and protocols were approved by MGH SRAC in accordance with the institutional animal ethics guidelines.

Cell Isolation and Culture

Lungs of mice were finely cut and digested with 1 mg/ml collagenase D (Roche) and 20 U/ml DNase I (Roche). Mouse lung fibroblasts were cultured in Dulbecco's modified Eagle's medium (DMEM), 15% FBS, 1% penicillin-streptomycin (P/S), NEAA, sodium pyruvate, HEPES, and L-glutamate. Spleens were homogenized and digested the same way, filtered through 70 μm cell strainer, and treated with red blood cell lysing buffer (Sigma-Aldrich). B, T, and dendritic cells were enriched by antibody-conjugated beads (Miltenyi). Mouse embryonic fibroblasts (*p53*-deficient) were subcultured (1:20) in DMEM with 10% FBS and 1% P/S.

DNA Content

Live cells were stained with Vybrant DyeCycle Ruby stain (Invitrogen) and fixed cells with PI at 50 μg/ml, 40 min, 37°C. Genomic DNA was isolated using GenElute mammalian genomic DNA miniprep kit (Sigma-Aldrich) for measurement by UV spectrophotometry.

Ara-C Experiment

For induction of DNA damage, we used 24 hr in vitro treatment of Ara-C at 10 μM or as indicated (Sigma-Aldrich). Sex-matched 10- to 12-week-old wild-type or *Dnase2a*$^{-/-}$ mice were untreated or injected i.p. with 3 consecutive doses of 15 μg/weight (g) Ara-C every 2 days. Weight and ankle thickness was measured at weeks 1, 2, 3, 4, 6, and 8 and compared to baseline at week 0. At the end of week 8, mice were euthanized, and tissues were dissected for hematoxylin and eosin staining and immunohistochemistry.

Dnase2a Rescue

Dnase2a ORF was cloned into a pCW57d-P2AR lentiviral Tet-on vector with puromycin resistance (The RNAi Consortium, Broad Institute). Plasmid DNA was purified and transfected into 293 cells for packaging of lentiviruses. *Dnase2a*$^{-/-}$ MLFs were infected with *Dnase2a* ORF or control eGFP virus, puromycin-selected (10 μg/ml) and seeded in 24-well plates for doxycycline induction (3 μg/ml, 24–48 hr). *Dnase2a* expression was confirmed by quantitative real-time PCR.

Knockdown Experiments

Cells were infected with puromycin-resistant lentiviral vector encoding shRNAs to *Dnase2a*, *Atg5*, or control or transfected with 150 nM of siGENOME pool siRNA (Dharmacon) targeting *Atg5*, *Tbk1*, *Sting*, or negative control, using Lipofectamine RNAiMAX (Life Technologies). Knockdown efficiency was confirmed by quantitative real-time PCR.

Immunofluorescence Cell Staining

We fixed cells with 4% PFA, permeabilized, blocked, and stained with antibodies against dsDNA (Santa Cruz Biotechnology), γ-H2AX, NUP98 (Cell Signaling Technology), LC3 (Novus Biologicals), and biotin-LAMP1 and BrdU (BioLegend), followed by fluorescent secondary antibodies or streptavidin. Images were captured using a Nikon eclipse ME600 fluorescence or Zeiss LMS510 confocal microscope, processed with NIS elements AR 2-30 or Carl Zeiss microimaging software, and analyzed with ImageJ across five to 20 random fields from at least two different experiments.

Live-Cell Imaging

Live-cell imaging was performed on MLFs grown on glass-bottom tissue culture dishes (FluroDish, World Precision Instruments) to reach 60%–80% confluence. Cell images were visualized using a spinning-disk confocal system (Ultraview confocal scanner, PerkinElmer) equipped with a Nikon Eclipse TE2000-U microscope and an environmental chamber (37°C, 5% CO_2) (Solent Scientific). Images were acquired with a plan APO TIRF Nikon oil immersion objective (60× 1.45) every 3–5 min for 2–8 hr using Z code stack. The images were processed with Volocity software (Volocity 6, PerkinElmer).

Please cite this article in press as: Lan et al., Dnase2a Deficiency Uncovers Lysosomal Clearance of Damaged Nuclear DNA via Autophagy, Cell Reports (2014), http://dx.doi.org/10.1016/j.celrep.2014.08.074

Statistical Analyses

All statistical analyses were performed using GraphPad PRISM 4 (GraphPad Software). All values were expressed as mean ± SEM. Samples were analyzed using Student's t test or as indicated, with $^{*}p < 0.05$, $^{**}p < 0.01$, and $^{***}p < 0.001$.

SUPPLEMENTAL INFORMATION

Supplemental Information includes Supplemental Experimental Procedures, six figures, and two movies and can be found with this article online at http://dx.doi.org/10.1016/j.celrep.2014.08.074.

AUTHOR CONTRIBUTIONS

Y.Y.L. and N.H. conceived the project, designed experimental strategies, and wrote the manuscript. D.L. performed, analyzed, and quantified histological and fluorescence imaging. R.B. performed the time-lapse imaging experiments. M.S.R. performed the computational analysis of DNA deep sequencing and assisted in statistics. All authors contributed to interpretation and discussion. Y.Y.L. performed all other experiments, and N.H. supervised the work.

ACKNOWLEDGMENTS

We thank S. Nagata and K. Kawane (Kyoto University) for *Dnase2a*-deficient mice; R. Xavier for *Atg5*$^{-/-}$ MEFs; F. Marangoni, F. Castelino, and N. Sakai for technical advice; W. Li, M. Roy, and M. Lee for technical help and reagents. We thank C. Vaziri for advice on DNA damaging agents. We thank R. Deering, T. Eisenhaure, M. Jovanovic, D.-A. Landau, M. Lee, K. Maciag, W. Pendergraft, and C. Villani of N.H.'s laboratory, for comments on the manuscript. We appreciate assistance of T.J. Diefenbach with confocal microscopy at the Ragon Institute Imaging Core; R. Mylvaganam with flow sorting at the Department of Pathology; M. McKee with electron microscopy at the Center for Systems Biology/Program in Membrane Biology, (supported by NIH DK43351 and DK57521); and the CCM staff for laboratory animal care. Y.Y.L. thanks M.A. Arnaout (T32 DK007540-22) and A.D. Luster (T32 AI060548-04, T32 AI060548-05) for training grant support. This work was supported by the NIH Director's New Innovator Award (DP2 OD002230) and the MGH Research Scholars Program to N.H.

Received: February 24, 2014
Revised: July 30, 2014
Accepted: August 28, 2014
Published: October 2, 2014

REFERENCES

Ahn, J., Gutman, D., Saijo, S., and Barber, G.N. (2012). STING manifests self DNA-dependent inflammatory disease. Proc. Natl. Acad. Sci. USA *109*, 19386–19391.

Barber, G.N. (2011). Cytoplasmic DNA innate immune pathways. Immunol. Rev. *243*, 99–108.

Barlow, J.H., Faryabi, R.B., Callén, E., Wong, N., Malhowski, A., Chen, H.T., Gutierrez-Cruz, G., Sun, H.W., McKinnon, P., Wright, G., et al. (2013). Identification of early replicating fragile sites that contribute to genome instability. Cell *152*, 620–632.

Barton, G.M., Kagan, J.C., and Medzhitov, R. (2006). Intracellular localization of Toll-like receptor 9 prevents recognition of self DNA but facilitates access to viral DNA. Nat. Immunol. *7*, 49–56.

Bass, B.P., Tanner, E.A., Mateos San Martín, D., Blute, T., Kinser, R.D., Dolph, P.J., and McCall, K. (2009). Cell-autonomous requirement for DNaseII in non-apoptotic cell death. Cell Death Differ. *16*, 1362–1371.

Blumenthal, A.B., and Clark, E.J. (1977). Discrete sizes of replication intermediates in Drosophila cells. Cell *12*, 183–189.

Brzostek-Racine, S., Gordon, C., Van Scoy, S., and Reich, N.C. (2011). The DNA damage response induces IFN. J. Immunol. *187*, 5336–5345.

Cai, H., Reinisch, K., and Ferro-Novick, S. (2007). Coats, tethers, Rabs, and SNAREs work together to mediate the intracellular destination of a transport vesicle. Dev. Cell *12*, 671–682.

Chowdhury, D., Beresford, P.J., Zhu, P., Zhang, D., Sung, J.S., Demple, B., Perrino, F.W., and Lieberman, J. (2006). The exonuclease TREX1 is in the SET complex and acts in concert with NM23-H1 to degrade DNA during granzyme A-mediated cell death. Mol. Cell *23*, 133–142.

Crow, Y.J., Hayward, B.E., Parmar, R., Robins, P., Leitch, A., Ali, M., Black, D.N., van Bokhoven, H., Brunner, H.G., Hamel, B.C., et al. (2006). Mutations in the gene encoding the 3′-5′ DNA exonuclease TREX1 cause Aicardi-Goutières syndrome at the AGS1 locus. Nat. Genet. *38*, 917–920.

Dauer, W.T., and Worman, H.J. (2009). The nuclear envelope as a signaling node in development and disease. Dev. Cell *17*, 626–638.

Delgado-Vega, A.M., Alarcón-Riquelme, M.E., and Kozyrev, S.V. (2010). Genetic associations in type I interferon related pathways with autoimmunity. Arthritis Res. Ther. *12* (*Suppl 1*), S2.

Drake, K.R., Kang, M., and Kenworthy, A.K. (2010). Nucleocytoplasmic distribution and dynamics of the autophagosome marker EGFP-LC3. PLoS ONE *5*, e9806.

Evans, C.J., and Aguilera, R.J. (2003). DNase II: genes, enzymes and function. Gene *322*, 1–15.

Ferguson, B.J., Mansur, D.S., Peters, N.E., Ren, H., and Smith, G.L. (2012). DNA-PK is a DNA sensor for IRF-3-dependent innate immunity. eLife *1*, e00047.

Gall, A., Treuting, P., Elkon, K.B., Loo, Y.M., Gale, M., Jr., Barber, G.N., and Stetson, D.B. (2012). Autoimmunity initiates in nonhematopoietic cells and progresses via lymphocytes in an interferon-dependent autoimmune disease. Immunity *36*, 120–131.

Galluzzi, L., Senovilla, L., Zitvogel, L., and Kroemer, G. (2012). The secret ally: immunostimulation by anticancer drugs. Nat. Rev. Drug Discov. *11*, 215–233.

Gómez, M., and Antequera, F. (2008). Overreplication of short DNA regions during S phase in human cells. Genes Dev. *22*, 375–385.

Graham, R.R., Hom, G., Ortmann, W., and Behrens, T.W. (2009). Review of recent genome-wide association scans in lupus. J. Intern. Med. *265*, 680–688.

Green, B.M., Finn, K.J., and Li, J.J. (2010). Loss of DNA replication control is a potent inducer of gene amplification. Science *329*, 943–946.

Hande, M.P., Balajee, A.S., Tchirkov, A., Wynshaw-Boris, A., and Lansdorp, P.M. (2001). Extra-chromosomal telomeric DNA in cells from Atm(-/-) mice and patients with ataxia-telangiectasia. Hum. Mol. Genet. *10*, 519–528.

Hasan, M., Koch, J., Rakheja, D., Pattnaik, A.K., Brugarolas, J., Dozmorov, I., Levine, B., Wakeland, E.K., Lee-Kirsch, M.A., and Yan, N. (2013). Trex1 regulates lysosomal biogenesis and interferon-independent activation of antiviral genes. Nat. Immunol. *14*, 61–71.

Hinz, M., Stilmann, M., Arslan, S.C., Khanna, K.K., Dittmar, G., and Scheidereit, C. (2010). A cytoplasmic ATM-TRAF6-cIAP1 module links nuclear DNA damage signaling to ubiquitin-mediated NF-κB activation. Mol. Cell *40*, 63–74.

Ikegami, S., Taguchi, T., Ohashi, M., Oguro, M., Nagano, H., and Mano, Y. (1978). Aphidicolin prevents mitotic cell division by interfering with the activity of DNA polymerase-alpha. Nature *275*, 458–460.

Ishii, K.J., and Akira, S. (2006). Innate immune recognition of, and regulation by, DNA. Trends Immunol. *27*, 525–532.

Ivanov, A., Pawlikowski, J., Manoharan, I., van Tuyn, J., Nelson, D.M., Rai, T.S., Shah, P.P., Hewitt, G., Korolchuk, V.I., Passos, J.F., et al. (2013). Lysosome-mediated processing of chromatin in senescence. J. Cell Biol. *202*, 129–143.

Iwasaki, A. (2012). A virological view of innate immune recognition. Annu. Rev. Microbiol. *66*, 177–196.

Kaiser, R., and Criswell, L.A. (2010). Genetics research in systemic lupus erythematosus for clinicians: methodology, progress, and controversies. Curr. Opin. Rheumatol. *22*, 119–125.

Kanda, T., Sullivan, K.F., and Wahl, G.M. (1998). Histone-GFP fusion protein enables sensitive analysis of chromosome dynamics in living mammalian cells. Curr. Biol. *8*, 377–385.

Kawane, K., Fukuyama, H., Kondoh, G., Takeda, J., Ohsawa, Y., Uchiyama, Y., and Nagata, S. (2001). Requirement of DNase II for definitive erythropoiesis in the mouse fetal liver. Science *292*, 1546–1549.

Kawane, K., Ohtani, M., Miwa, K., Kizawa, T., Kanbara, Y., Yoshioka, Y., Yoshikawa, H., and Nagata, S. (2006). Chronic polyarthritis caused by mammalian DNA that escapes from degradation in macrophages. Nature *443*, 998–1002.

Kawane, K., Tanaka, H., Kitahara, Y., Shimaoka, S., and Nagata, S. (2010). Cytokine-dependent but acquired immunity-independent arthritis caused by DNA escaped from degradation. Proc. Natl. Acad. Sci. USA *107*, 19432–19437.

Kawashima, A., Tanigawa, K., Akama, T., Wu, H., Sue, M., Yoshihara, A., Ishido, Y., Kobiyama, K., Takeshita, F., Ishii, K.J., et al. (2011). Fragments of genomic DNA released by injured cells activate innate immunity and suppress endocrine function in the thyroid. Endocrinology *152*, 1702–1712.

Ko, A., Kanehisa, A., Martins, I., Senovilla, L., Chargari, C., Dugue, D., Mariño, G., Kepp, O., Michaud, M., Perfettini, J.L., et al. (2014). Autophagy inhibition radiosensitizes in vitro, yet reduces radioresponses in vivo due to deficient immunogenic signalling. Cell Death Differ. *21*, 92–99.

Kobiyama, K., Takeshita, F., Jounai, N., Sakaue-Sawano, A., Miyawaki, A., Ishii, K.J., Kawai, T., Sasaki, S., Hirano, H., Ishii, N., et al. (2010). Extrachromosomal histone H2B mediates innate antiviral immune responses induced by intracellular double-stranded DNA. J. Virol. *84*, 822–832.

Kondo, T., Kobayashi, J., Saitoh, T., Maruyama, K., Ishii, K.J., Barber, G.N., Komatsu, K., Akira, S., and Kawai, T. (2013). DNA damage sensor MRE11 recognizes cytosolic double-stranded DNA and induces type I interferon by regulating STING trafficking. Proc. Natl. Acad. Sci. USA *110*, 2969–2974.

Krick, R., Muehe, Y., Prick, T., Bremer, S., Schlotterhose, P., Eskelinen, E.L., Millen, J., Goldfarb, D.S., and Thumm, M. (2008). Piecemeal microautophagy of the nucleus requires the core macroautophagy genes. Mol. Biol. Cell *19*, 4492–4505.

Krieser, R.J., MacLea, K.S., Longnecker, D.S., Fields, J.L., Fiering, S., and Eastman, A. (2002). Deoxyribonuclease IIalpha is required during the phagocytic phase of apoptosis and its loss causes perinatal lethality. Cell Death Differ. *9*, 956–962.

Lee-Kirsch, M.A., Gong, M., Chowdhury, D., Senenko, L., Engel, K., Lee, Y.A., de Silva, U., Bailey, S.L., Witte, T., Vyse, T.J., et al. (2007). Mutations in the gene encoding the 3′-5′ DNA exonuclease TREX1 are associated with systemic lupus erythematosus. Nat. Genet. *39*, 1065–1067.

Mazur, D.J., and Perrino, F.W. (2001). Excision of 3′ termini by the Trex1 and TREX2 3′—>5′ exonucleases. Characterization of the recombinant proteins. J. Biol. Chem. *276*, 17022–17029.

Mijaljica, D., Prescott, M., and Devenish, R.J. (2010). The intricacy of nuclear membrane dynamics during nucleophagy. Nucleus *1*, 213–223.

Morita, M., Stamp, G., Robins, P., Dulic, A., Rosewell, I., Hrivnak, G., Daly, G., Lindahl, T., and Barnes, D.E. (2004). Gene-targeted mice lacking the Trex1 (DNase III) 3′—>5′ DNA exonuclease develop inflammatory myocarditis. Mol. Cell. Biol. *24*, 6719–6727.

Nagai, S., Dubrana, K., Tsai-Pflugfelder, M., Davidson, M.B., Roberts, T.M., Brown, G.W., Varela, E., Hediger, F., Gasser, S.M., and Krogan, N.J. (2008). Functional targeting of DNA damage to a nuclear pore-associated SUMO-dependent ubiquitin ligase. Science *322*, 597–602.

Napirei, M., Karsunky, H., Zevnik, B., Stephan, H., Mannherz, H.G., and Möröy, T. (2000). Features of systemic lupus erythematosus in Dnase1-deficient mice. Nat. Genet. *25*, 177–181.

Novakova, Z., Hubackova, S., Kosar, M., Janderova-Rossmeislova, L., Dobrovolna, J., Vasicova, P., Vancurova, M., Horejsi, Z., Hozak, P., Bartek, J., and Hodny, Z. (2010). Cytokine expression and signaling in drug-induced cellular senescence. Oncogene *29*, 273–284.

Oza, P., Jaspersen, S.L., Miele, A., Dekker, J., and Peterson, C.L. (2009). Mechanisms that regulate localization of a DNA double-strand break to the nuclear periphery. Genes Dev. *23*, 912–927.

Ozeri-Galai, E., Bester, A.C., and Kerem, B. (2012). The complex basis underlying common fragile site instability in cancer. Trends Genet. *28*, 295–302.

Paludan, S.R., and Bowie, A.G. (2013). Immune sensing of DNA. Immunity *38*, 870–880.

Pang, D., Winters, T.A., Jung, M., Purkayastha, S., Cavalli, L.R., Chasovkikh, S., Haddad, B.R., and Dritschilo, A. (2011). Radiation-generated short DNA fragments may perturb non-homologous end-joining and induce genomic instability. J. Radiat. Res. (Tokyo) *52*, 309–319.

Park, Y.E., Hayashi, Y.K., Bonne, G., Arimura, T., Noguchi, S., Nonaka, I., and Nishino, I. (2009). Autophagic degradation of nuclear components in mammalian cells. Autophagy *5*, 795–804.

Park, J.S., Lim, M.A., Cho, M.L., Ryu, J.G., Moon, Y.M., Jhun, J.Y., Byun, J.K., Kim, E.K., Hwang, S.Y., Ju, J.H., et al. (2013). p53 controls autoimmune arthritis via STAT-mediated regulation of the Th17 cell/Treg cell balance in mice. Arthritis Rheum. *65*, 949–959.

Rello-Varona, S., Lissa, D., Shen, S., Niso-Santano, M., Senovilla, L., Mariño, G., Vitale, I., Jemaá, M., Harper, F., Pierron, G., et al. (2012). Autophagic removal of micronuclei. Cell Cycle *11*, 170–176.

Robert, T., Vanoli, F., Chiolo, I., Shubassi, G., Bernstein, K.A., Rothstein, R., Botrugno, O.A., Parazzoli, D., Oldani, A., Minucci, S., and Foiani, M. (2011). HDACs link the DNA damage response, processing of double-strand breaks and autophagy. Nature *471*, 74–79.

Roberts, P., Moshitch-Moshkovitz, S., Kvam, E., O'Toole, E., Winey, M., and Goldfarb, D.S. (2003). Piecemeal microautophagy of nucleus in Saccharomyces cerevisiae. Mol. Biol. Cell *14*, 129–141.

Saitoh, T., Fujita, N., Hayashi, T., Takahara, K., Satoh, T., Lee, H., Matsunaga, K., Kageyama, S., Omori, H., Noda, T., et al. (2009). Atg9a controls dsDNA-driven dynamic translocation of STING and the innate immune response. Proc. Natl. Acad. Sci. USA *106*, 20842–20846.

Settembre, C., Fraldi, A., Jahreiss, L., Spampanato, C., Venturi, C., Medina, D., de Pablo, R., Tacchetti, C., Rubinsztein, D.C., and Ballabio, A. (2008). A block of autophagy in lysosomal storage disorders. Hum. Mol. Genet. *17*, 119–129.

Shoji, J.Y., Kikuma, T., Arioka, M., and Kitamoto, K. (2010). Macroautophagy-mediated degradation of whole nuclei in the filamentous fungus Aspergillus oryzae. PLoS ONE *5*, e15650.

Sogo, J.M., Lopes, M., and Foiani, M. (2002). Fork reversal and ssDNA accumulation at stalled replication forks owing to checkpoint defects. Science *297*, 599–602.

Stetson, D.B., and Medzhitov, R. (2006). Recognition of cytosolic DNA activates an IRF3-dependent innate immune response. Immunity *24*, 93–103.

Stetson, D.B., Ko, J.S., Heidmann, T., and Medzhitov, R. (2008). Trex1 prevents cell-intrinsic initiation of autoimmunity. Cell *134*, 587–598.

Sugihara, T., Murano, H., Nakamura, M., Ichinohe, K., and Tanaka, K. (2011). Activation of interferon-stimulated genes by gamma-ray irradiation independently of the ataxia telangiectasia mutated-p53 pathway. Mol. Cancer Res. *9*, 476–484.

Watson, R.O., Manzanillo, P.S., and Cox, J.S. (2012). Extracellular M. tuberculosis DNA targets bacteria for autophagy by activating the host DNA-sensing pathway. Cell *150*, 803–815.

Yang, Y.G., Lindahl, T., and Barnes, D.E. (2007). Trex1 exonuclease degrades ssDNA to prevent chronic checkpoint activation and autoimmune disease. Cell *131*, 873–886.

Yang, Y., Xia, F., Hermance, N., Mabb, A., Simonson, S., Morrissey, S., Gandhi, P., Munson, M., Miyamoto, S., and Kelliher, M.A. (2011). A cytosolic ATM/NEMO/RIP1 complex recruits TAK1 to mediate the NF-kappaB and p38 mitogen-activated protein kinase (MAPK)/MAPK-activated protein 2 responses to DNA damage. Mol. Cell. Biol. *31*, 2774–2786.

Yasutomo, K., Horiuchi, T., Kagami, S., Tsukamoto, H., Hashimura, C., Urushihara, M., and Kuroda, Y. (2001). Mutation of DNASE1 in people with systemic lupus erythematosus. Nat. Genet. *28*, 313–314.

Yoshida, H., Okabe, Y., Kawane, K., Fukuyama, H., and Nagata, S. (2005). Lethal anemia caused by interferon-beta produced in mouse embryos carrying undigested DNA. Nat. Immunol. *6*, 49–56.

Zhang, X., Brann, T.W., Zhou, M., Yang, J., Oguariri, R.M., Lidie, K.B., Imamichi, H., Huang, D.W., Lempicki, R.A., Baseler, M.W., et al. (2011). Cutting edge: Ku70 is a novel cytosolic DNA sensor that induces type III rather than type I IFN. J. Immunol. *186*, 4541–4545.